ECCOMAS Congress 2016
VII European Congress on Computational Methods in Applied Sciences and Engineering
M. Papadrakakis, V. Papadopoulos, G. Stefanou, V. Plevris (eds.)
Crete Island, Greece, 5–10 June 2016

NUMERICAL AND EXPERIMENTAL INVESTIGATIONS OF DYNAMIC STALL PROBLEM ON A 2D HELICOPTER ROTOR BLADE SECTION

A. Marino[1], S. Russo[2], G. P. Reina[3], G. Esposito[1], F. Capizzano[1], C. de Nicola[2]

[1] Italian Aerospace Research Center
Aircraft Department
Via Maiorise snc
81043, Capua (CE), Italy
e-mail: f.capizzano@cira.it, a.marino@cira.it, web page: http://www.cira.it

[2] Università degli Studi di Napoli Federico II - Scuola Politecnica e delle Scienze di Base
Dipartimento di Ingegneria Chimica, dei Materiali e della Produzione Industriale
Piazzale V. Tecchio, 80
80125, Napoli, Italy
e-mail: aneres85@gmail.com, denicola@unina.it

[3] Seconda Università degli Studi di Napoli - Scuola Politecnica e delle Scienze di Base
Dipartimento di Ingegneria Industriale e dell'Informazione
Via Roma, 29
81031 Aversa (CE), Italy
e-mail: giovannipaolo.reina@unina2.it

Keywords: Dynamic Stall, Rotor Blade Section, Gurney Flap.

Abstract. *This work deals with the effects of an Active Gurney Flap device on the aerodynamic performance of oscillating rotor blade sections in different incidence ranges (pre-stall and dynamic stall conditions). Numerical and experimental simulations are carried out for different flow conditions, airfoil oscillation characteristics and Gurney flap activation laws, in order to assess the potential benefits of such a device on controlling blade loads and to get a deeper insight on the involved flow phenomena. This document is focused on the numerical simulation methodology and associated results obtained for some relevant cases selected from the wind-tunnel experiments test matrix.*

1 INTRODUCTION

Huge efforts have been dedicated to improve the performance of aircraft systems, including propulsion systems, propellers as well as aerodynamics systems. The main objectives are better efficiency, reduced fuel consumption and corresponding environmental gains. For helicopters, blade morphing technologies have become of interest to reduce noise and vibrations.

The study of the dynamic stall phenomenon on the rotor blade represents one of the major research topics in helicopter aerodynamics. The first analysis of the dynamic stall effects on helicopter rotor blades appeared in an experimental study in 1960 (see [1]). Empirical techniques were developed ([1][2]) that attempted to represent the primary effects of dynamic stall on airfoil lift and pitching-moment characteristics. Parametric experiments were run to expand the database used for improving these empirical methods ([3][4] [5]). The experiments were primarily directed toward obtaining aerodynamic force and moment coefficients as functions of frequency and angle, and the empirical corrections, which developed from these tests, were the prime source for improving helicopter aerodynamic prediction methods. The first investigation which attempted to isolate the fluid dynamic phenomena causing dynamic stall led to a correlation between experimental pressure distributions and the movement of a strong vortex along the surface of the airfoil ([6][7]). The presence of this vortex that forms on the upper surface of the airfoil can produce lift significantly greater than that obtained in steady flow ([8][9]) and dramatic changes in the lift and moment characteristics of the airfoil ([10]). The main consequence of these phenomena is a hysteresis loop developed in both lift and pitching moments with much larger magnitudes developed than in steady flow. At the end of the cycle, when the vortex leaves the airfoil, there is an abrupt drop in lift and moment.

This fact gives strong limitations for the operational envelope of helicopters during maneuvers, high-speed flight, and operations at high density-altitude. For all these reasons, several research activities are ongoing to control/delay the rotor blade dynamic stall. Improvements rely upon the optimization of the blade airfoil shape, or, as alternative, adopting active/passive systems. Due to the strong demand for faster helicopters/blade, in recent years, the dynamic stall phenomenon has become one of the more investigated topics in aerodynamic and aeroelasticity fields. Several research activities both in experimental and numerical fields are currently focused on the design and development of advanced rotor blades equipped with active and passive devices to mitigate the detrimental effects on the helicopter performance produced by the dynamic stall on the retreating side of the rotor ([11]).

Between a range of potential technologies that could be incorporated within active segments of a helicopter main rotor blade, the ‘Active Gurney Flap’ (AGF) seems to be the most interesting solution. The AGF is a small appendix perpendicular to the surface of the airfoil (typically on the lower surface) with the ability to alter its height from zero (fully retracted) to a maximum value (fully protruded). The AGF concept is attracting more and more interest because of its relatively low power demand and stronger resistance to blade centrifugal stresses when compared to other similar active devices. To assess the potential benefits deriving from the use of AGF on smart rotors in forward flight, as well as to mature the knowledge in the field of the complex unsteady phenomena involved, the development of adequate numerical and experimental tools is required, providing methodologies able to estimate the AGF influence on aerodynamic blade loads.

In the last 20 years, several wind tunnel facilities have been upgradated/modified to allow simulating the unsteady flow conditions around pitch oscillating airfoils. The most recent experimental research activities have been performed in the DNW-TWG transonic wind tunnel facility located at DLR-Göttingen, Germany (see [12][13]) or in the Icing Research Tunnel

(IRT) at the NASA Glenn Research Center ([14]). One of the major limit of the existing WT facilities is that they are able to cover only a limited "Mach-Reynolds-Pitching Reduced frequency" operative envelope with respect to the typical flight conditions of helicopters. With this work, we propose to reproduce, in CIRA Icing Wind Tunnel Test facility, Deep Dynamic Stall conditions acting on a full-scale retreating rotor blade section referred to a medium size helicopter (NH90 like) and analyze the effect of AGF devices on the performances of the airfoil. Moreover the experimental results will be compared with numerical data of computational fluid dynamic simulations.

This paper contains a description of the experimental apparatus able to simulate Deep Dynamic Stall situations and numerical results. It is structured as follow. Section 2 deals with a description of the Experimental Set-Up, including some details about the pitch oscillating airfoil and the characteristics of CIRA Icing Wind Tunnel. Section 3 is devoted to the Numerical Results founded in different flight conditions. Finally, Section 4 contains the Conclusions.

2 EXPERIMENTAL SET-UP

2.1 The Pitch Oscillating Airfoil

The pitch-oscillating system is composed by a wall-to-wall full span model (1.1m) having a NACA 0018 airfoil section and a chord of 0.28m. It is activated by one power system (electric motor) with a reduction gear system able to generate the required pitch-oscillation motion around the model quarter-chord axis. The model is integrated in the wind tunnel test section by means of two interface disks, for each side of the test section, one connected to the pitch-oscillating motor and the other to a mechanical support. A general view of the pitch-oscillating system is reported in Figure 1.

From a technical point of view, according with the given requirements, the pitch-oscillating system has been designed to generate a pitch-oscillating motion of the 2D model with the following laws:

$$\alpha = \alpha_M - \alpha_0 \sin(\omega t)$$

where α_M, α_0 and ω are, respectively, the mean angle, the oscillating angle and the angular velocity.

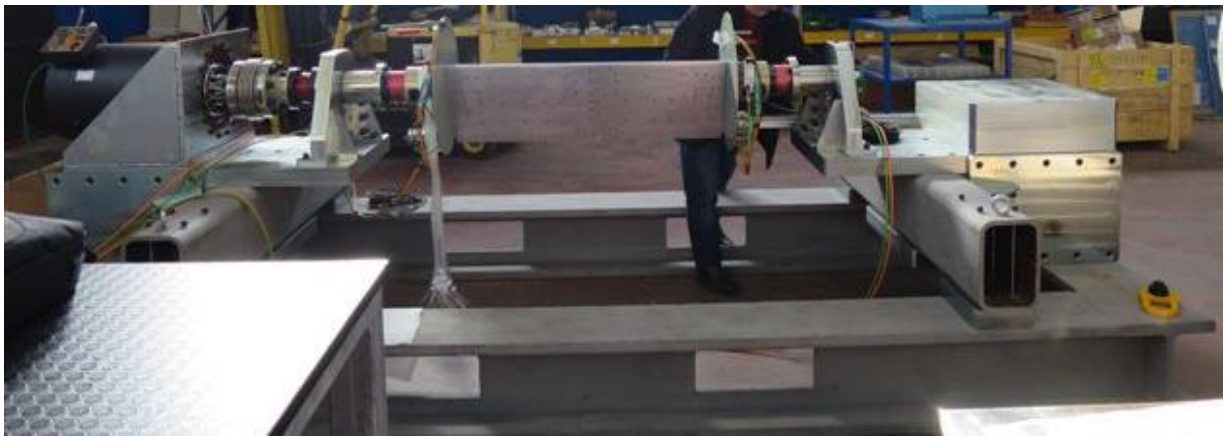

Figure 1: P*itch-oscillating system*

The system is integrated in the Secondary Test Section (STS) of the CIRA Icing Wind Tunnel (IWT). Officially inaugurated in September 2002, the IWT is one of the most advanced ground facilities for aerodynamic tests in icing conditions. The IWT is a closed loop-circuit, refrigerated, pressurized aerodynamic and icing wind tunnel equipped with four interchangeable test sections able to reproduce the atmospheric conditions up to a height of 7000 m and static temperature of -40°C. The test section can have both closed or slotted walls with 7% open area. Airflow refrigeration is obtained via a twin row heat exchanger; the minimum achievable static temperature in the STS is –40°C. In addition, an evacuation/pressurization air system allows static pressure being regulated between 39,000 Pa, corresponding to an altitude of about 7,000 m, and 145,000 Pa, for high Reynolds number aerodynamic tests.

The Pitching oscillating test rig is interfaced to the STS-Secondary Test Section frame (height 2.35m, width 1.15m, length 5.0m) allowing tests up to M=0.7. Figure 2 shows a general view of the IWT facility and of the STS. The details of the IWT facility and its operative envelope are provided in [15]**.**

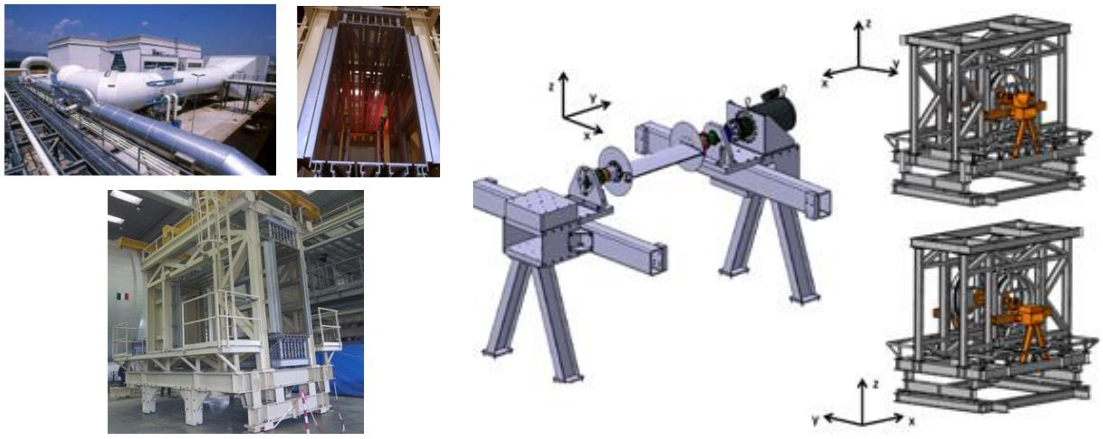

Figura 2: General View of the IWT (up/left and down) and view of the STS (right)

2D pitch oscillating tests will be performed on a NACA0018 airfoil having a chord length of 0.28m having a wing span length of 1.15m to be installed in wind tunnel in the "wall to wall" configuration. The 2D WT model has been designed to meet an adequate structural integrity under aerodynamic and inertial loads as well as model modularity to allow the setting of the different configurations. An overview of the 2D model is reported in Figure 3. The airfoil has been designed to guarantee sufficient access to the instrumentation installed inside the model, by minimizing the number of removable components and mitigating the risk of steps, gaps and/or imperfections on external skin, which can affect the natural flow development. At this regard, removable panels have been manufactured on the lower part of the surface, by leaving the upper surface of the model clean. The model has been designed to allow different configurations:

- Clean configuration (absence of GF);
- No. 2 model configurations having a fixed GF with 1.4 % and 2.8 % of protrusion length respectively, with GF located on the lower surface at 95% of the model chord.

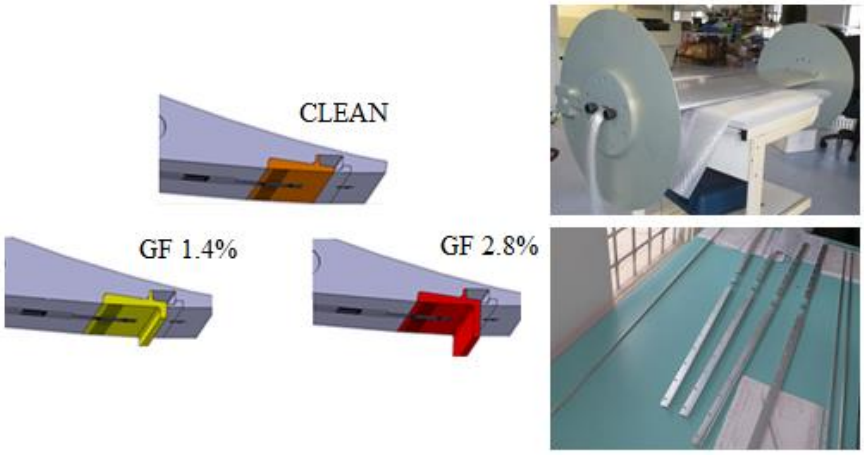

Figure 3: 2D Wind Tunnel Model Configurations

3 NUMERICAL SIMULATIONS

This section is devoted to the numerical study of the aerodynamic behavior of a NACA 0018 airfoil without and with a fixed Gurney Flap. First of all a description of the geometrical data and operating conditions is presented; then steady and unsteady results are detailed.

3.1 Geometrical data and selected operating conditions

The analyzed blade section is represented by a NACA 0018 airfoil (see [16] for coordinates set). For the present calculations, a blade section chord of 0.28 meters is considered and the airfoil angle of incidence is time-modulated according to the following harmonic oscillation law

$$\boldsymbol{\alpha = \alpha_M - \alpha_0 \sin(2\pi f t)}$$

where f is the frequency of pitch oscillations.
Computations include both steady and unsteady simulations according to Table 1, which represents the wind tunnel test matrix selected for cross-comparison of numerical predictions against experimental results.

Blade Motion	**Mach Number**	**Reynolds Number**	$\boldsymbol{\alpha_M}$	$\boldsymbol{\alpha_0}$	**f**	**AGF**
Fixed Airfoil	0.3	1×10^6	$[-2° \rightarrow 20°]$	0	N/A	OFF
						FIXED (1.4-2.8%)
Rotating Airfoil	0.3	1×10^6	8°	6°	3 Hz	OFF
						FIXED (1.4-2.8%)

Table 1: Summary of numerical simulations

The Gurney Flap device is positioned on the lower side of the airfoil, at 95% of the chord, and it reaches a maximum protrusion length equal to 1.4% and 2.8% of the chord (i.e. 4 or 8 mm). Unsteady simulations are also performed for the oscillating airfoil with Gurney Flap device fully extended during the whole pitch cycle (fixed protrusion length).

3.2 Domain discretization and boundary conditions

The fluid domain has a typical C-shape with outer boundaries located 30 chord length away from the body surface. The minimum spacing in the normal direction to the airfoil surface is set to an adequate value to solve the boundary layer down to the airfoil surface (unitary dimensionless wall distance with growth ratio around 1). Figure 4 shows a sketch of the leading edge grid on the airfoil.

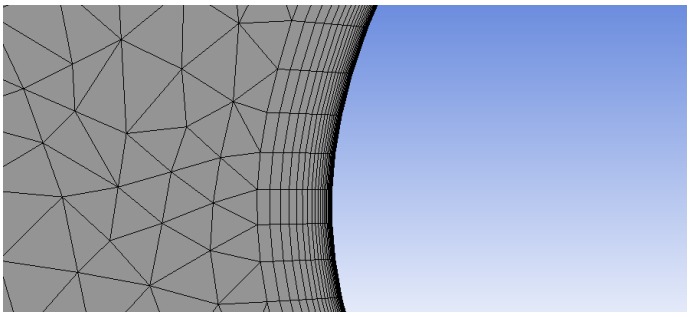

Figure 4: Mesh close–up view

All flow simulations listed in Table 1 use the same computational mesh and boundary conditions: cases with extended Gurney Flap (fixed length) are computed applying a solid wall boundary condition to both faces lying on the GF surface.

3.3 Flow solver and CFD approach

The Reynolds–Averaged Navier-Stokes equations are solved with a finite volume method (FV), so they are expressed as a system of conservation laws that relate rate of mass change, momentum, and energy in a control volume of area A to the spatial fluxes of these quantities through the volume. The flow field is computed using the commercial CFD code ANSYS Fluent R15.0. The presented computations solve URANS equations using a k-ω SST turbulence closure (see [18]) for all cases. According to the wind-tunnel model set-up, CFD simulations were run as fully turbulent, i.e. with no transition model and no regions with artificially modified turbulence production.

The novel element of this work is the application of the dynamic meshing methodology to obtain accurate time-dependent results because the computational mesh varies in time consistently with the changing positions of the different moving bodies. This dynamic approach allows the numerical solution to more closely follow the unsteady flow evolution and, thus, to better represent the time history of the forces acting on the bodies surfaces (see [19]). In order to avoid the deterioration of the mesh quality and/or the degeneration of existing FV cells, due to the geometry modification, two different methods are used, which are referred to as “smoothing” and “remeshing”. The former technique consists in moving the interior nodes of the mesh without changing their number and their connectivity. The latter technique allows for the local update of the mesh by either adding or deleting cells, where the boundary displacement would be

otherwise too large with respect to the local mesh size. After some preliminary tests demonstrating the feasibility of such an approach, the remeshing and the spring–based smoothing techniques are simultaneously used in the present work.

3.4 Results

A preliminary characterization of the airfoil aerodynamic performances at fixed incidence angles (fixed airfoil conditions) is performed to compare our numerical predictions with both available data from other experimental and numerical set-up and, so, to provide reference data for unsteady computations. Figure 5 depicts the trend of the lift coefficient against the angle of attack: our data (black curve) are compared with [20], [21] and [22]. The agreement between our results and the experimental data is good, especially in the linear part of the curve.

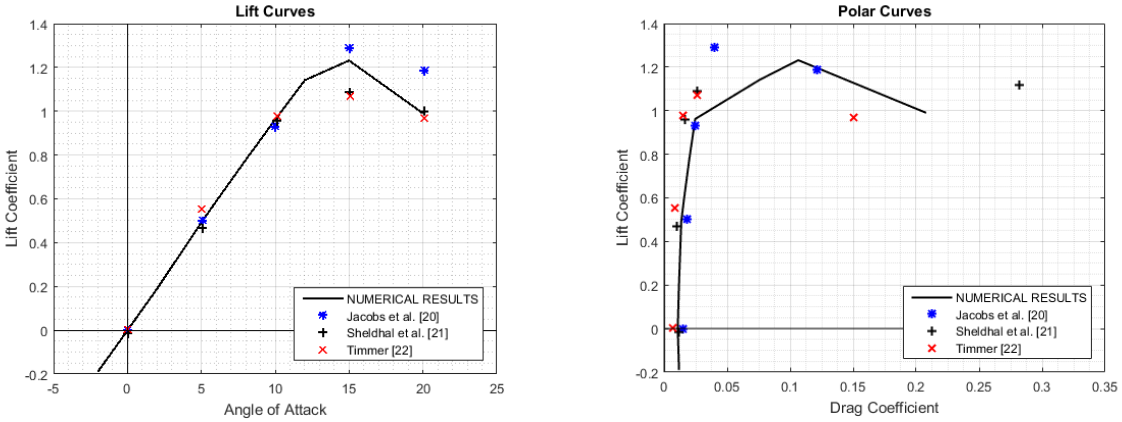

Figura 5: Lift and Polar Curves

Figures 7 and 8 refer to the cases in which the Gurney Flap assumes fixed positions. Watching the $C_l(\alpha)$ curve (Figure 6), it is noticeable, respectively, an increasing of 6% and 8% of the C_l for the model with the 1.4% and 2.8% fixed Gurney flap in comparison with the clean configuration. Moreover, the stall angle diminishes from 15 deg to 12 deg. The $C_l(\alpha)$ slope doesn't show significant changes in comparison with the clean airfoil.

Comparing the $C_d(\alpha)$ curves (see Figure 7), a section drag increment is observed along the curve being more important in the range of high angles of attack. There is also a 10% increment

of the C_{d0} in comparison with the clean airfoil. All of these conclusions have a good agreement with other papers focused on the same topic (see [23], [24]).

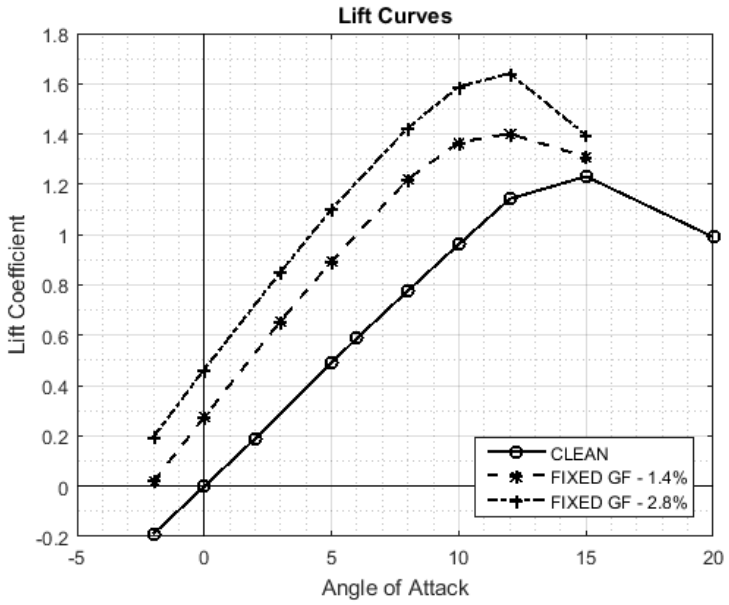

Figure 6: Lift curves

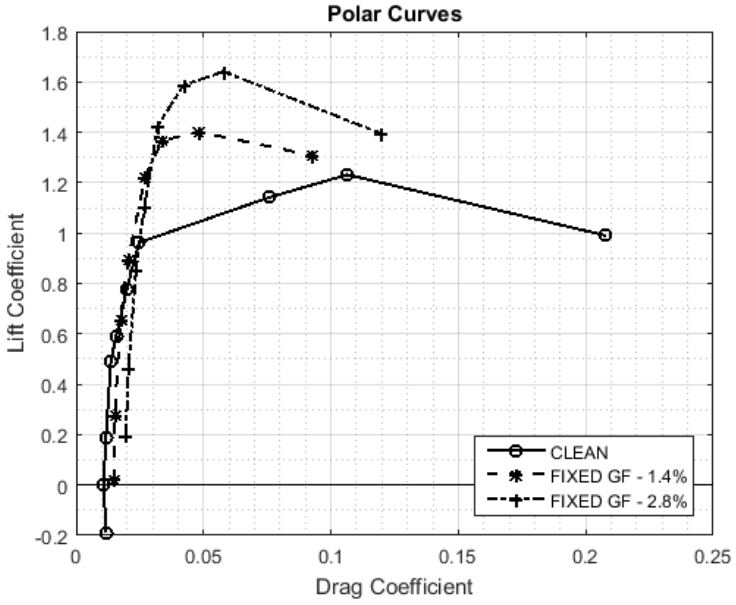

Figure 7: Polar curves

Figure 8 shows the trend of the pressure coefficient at $C_l = 0.78$. The main difference is the presence of a plateau of pressure in the rear part of the airfoil after the GF. Moreover the presence of small humps in the pressure coefficient for all configurations denotes the existence of laminar bubbles on the upper side of the airfoil. This fact is also confirmed by data presented in literature ([16]).

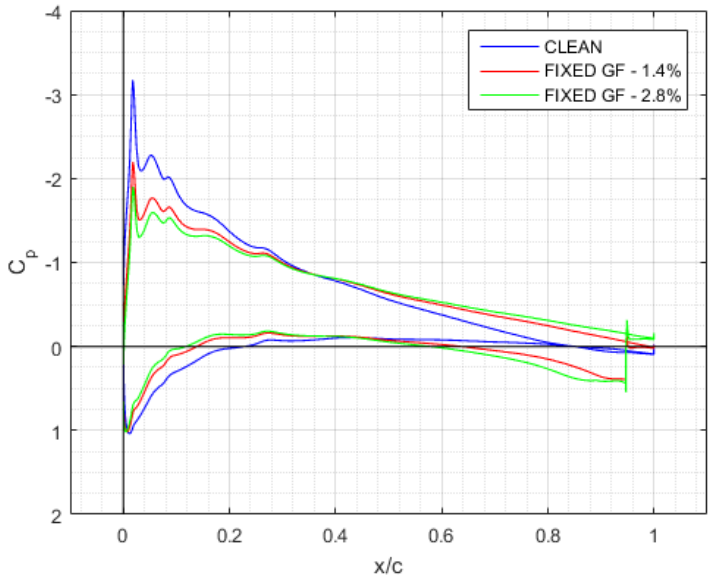

Figura 8: Pressure Coefficient ($C_l = 0.78$)

Figure 9 shows the comparison between the oscillating case and the corresponding steady case, for the configuration with 1.4% fixed Gurney Flap. As we expect, the maximum lift coefficient in the oscillating case is greater than that of the fixed case. In this case the Light Dynamic Stall is exploring in which the maximum angle of oscillation is not so far from the steady one.

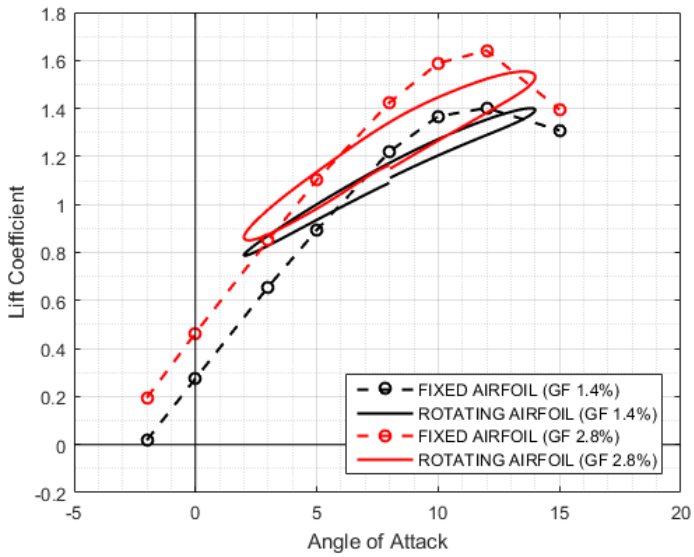

Figure 9: Lift Curves

4 CONCLUSIONS

This work addresses the characterization of the aerodynamics of the Gurney Flap from the experimental and numerical point of view. The first part describes the experimental apparatus to study Dynamic Stall conditions acting on a full-scale retreating rotor blade section referred to a medium size helicopter. In the second part, numerical results are performed in both static and dynamic configurations: all of them have demonstrated the capability of GF devices in increasing the maximum lift coefficient and, so, alleviating some negative aspects of the dynamic stall. Dynamic simulations are focused on the Light Dynamic Stall problem, in which the maximum angle of oscillation is not so far from the steady one.

4.1 Future works

A future extension of this work will contain the results of the experimental tests into two different conditions: clean and with fixed GF configurations. These results will be compared with the numerical simulations of this paper. In addition to the Light Dynamic Stall, next calculations will be focused on the characterization of the Deep Dynamic Stall in which the maximum angle achieved during the oscillation is much higher with respect to the Light Stall. Simulations will be, also, performed on an oscillating airfoil having an active Gurney Flap.

Future developments regarding the experimental apparatus will be the integration of an active Gurney Flap device in the pitching oscillating test rig.

REFERENCES

[1] F. O. Carta, Experimental Investigation of the Unsteady Aerodynamic Characteristics of a NACA 0012 Airfoil, *UAC RL Report M-1283-1*, July 26, 1960.

[2] F. D. Harris, R. R. Pruyn, Blade Stall – Half Fact, Half Fiction. *J. Amer. Helicopter Soc*., Vol. 13, No. 2, 1968, pp. 27-48.

[3] J. Liiva, F.J. Davenport, L. Gray, I. C. Walton, Two-Dimensional Tests of Airfoils Oscillating Near Stall, *U.S. Army AVLABS, TR68-13*, 1968.

[4] L. Gray, J. Liiva, F. J. Davenport, Wind-Tunnel Tests of Thin Airfoils Oscillating Near Stall. *U.S. Army AVLABS, TR68-89A*, 1969.

[5] R. I. Windsor: Measurement of Aerodynamic Forces on an Oscillating Airfoil, *U. S. Army AVLABS TR69-98*, 1970.

[6] M. S. Garelick, Non-Steady Airloads on Dynamically Stalling Two-Dimensional Wings. *Master's Degree Thesis*, MIT, 1967.

[7] N.D. Ham, M.S. Garrelick, Dynamic Stall Considerations in Helicopter Rotors. *J. Amer. Helicopter Soc.*, Vol. 13, 1968, pp. 49-55.

[8] McAlister, K. W., and McCroskey, W. J., Analysis of the Development of Dynamic Stall Based on Oscillating Airfoil Experiments, *NASA TN-8382*, Jan. 1977.

[9] Carr, L. W, Progress in Analysis and Prediction of Dynamic Stall, *Journal of Aircraft*, Vol. 25, No. 1, 1988, pp. 6-17.

[10] Carr, L. W., M. S. Chandrasekharat, Design and Development of a Compressible Dynamic Stall Facility, *Journal of Aircraft* Vol. 29, No. 3, May-June 1992

[11] H. Mai, G. Dietz, W. Geissler, et al. Dynamic stall control by leading edge vortex generators, *J. Am. Helicopter. Soc.*, 2008; 56: 26–36.

[12] W. Geissler and al., Dynamic Stall Control Investigations on a Full Size Chord Blade Section, *European Rotorcraft Forum*, 2004

[13] Dynamic Stall and its Passive Control Investigations on the OA209 Airfoil Section, *31th European Rotorcraft Forum*, 2014

[14] T. Reinert and al., Oscillating Airfoil Icing Tests in the NASA Glenn Research Center Icing Research Tunnel, *2011-38-0016 SAE International*, 2011

[15] "Cira Icing Wind Tunnel User Manual", www.cira.it.

[16] I. H. Abbott, A. E. von Doenhoff, Theory of Wing Sections: Including a Summary of Airfoil Data. *Dover Books*, 1945.

[17] J.H. Argyris, M. Papadrakakis, L. Karapitta, Elastoplastic analysis of shells with the triangular element TRIC. M. Papadrakakis, A. Samartin, E. Oñate eds. *4th International Colloquium on Computation of Shell and Spatial Structures (IASS-IACM 2000)*, Chania, Crete, Greece, June 4-7, 2000.

[18] F. R. Menter, Two Equation Eddy Viscosity Turbulence Models for Engineering Applications. *AIAA Journal*, **32**, 1598–1605, 1994.

[19] S. Russo, G. P. Reina, C. de Nicola. RANS prediction of the flap unsteady aerodynamics using dynamic mesh. *Memories XXV Congresso AIDAA Torino*, 17-19 November (2015).

[20] E. Jacobs, N. A. Sherman, Airfoil section characteristics as affected by variations of the Reynolds number. *NACA Report 586*, 1937

[21] R. E. Shedahl, and P. C Klimas, Aerodynamic characteristics of seven airfoil sections through 180 degrees angle of attack for use in aerodynamic analysis of vertical axis wind turbines, *Technical Report No. SAND80-2114*, 1981

[22] W.A. Timmer, Two-dimensional low-Reynolds number wind tunnel results for airfoil NACA 0018, *Wind Engineering*, 32(6), pp. 525–537, 2008

[23] M. E. Camocardi, J. M. Di Leo, J. S. Delnero, J. L. Colman Lerner, Experimental Study Of A Naca 4412 Airfoil With Movable Gurney Flap, *49th AIAA Aerospace Sciences Meeting*, 4 - 7 January 2011, Orlando, Florida, 2011

[24] D. Tang, E. H. Dowell, Aerodynamic Loading for an Airfoil with an Oscillating Gurney Flap, *JOURNAL OF AIRCRAFT*, Vol. 44, N. 4, 2007